physica status solidi b

www.pss-b.com

Correlation of the Carrier Decay Time and Barrier Thickness for Asymmetric Cubic GaN/$Al_{0.64}Ga_{0.36}N$ Double Quantum Wells

Tobias Wecker, Gordon Callsen, Axel Hoffmann, Dirk Reuter, and Donat J. As*

The carrier transfer via non-resonant tunneling is of great significance for many devices like the quantum cascade laser. In this study time-resolved photoluminescence is used for an investigation of this effect in asymmetric double quantum wells for low temperatures. The Al content in these asymmetric double quantum wells was determined by HRXRD to $x = 0.64 \pm 0.03$. The growth of the asymmetric cubic GaN/$Al_xGa_{1-x}N$ double quantum wells was performed by a radio-frequency plasma-assisted molecular beam epitaxy. As a substrate, 3C-SiC (001) on top of Si (001) was used. Three samples with different barrier thickness d were analysed (1 nm, 3 nm, 15 nm). The two quantum wells are designed with the thicknesses 2.5 nm and 1.35 nm. Thus, three expected emission bands measured in luminescence can be resolved. The maximum intensities are 3.49 eV (wide well), 3.73 eV (narrow well) and 4.12 eV (AlGaN). A correlation between the carrier lifetimes of the quantum wells (QWs) and the barrier width is found. Exploiting rate equations, the intensity ratio of both QW emissions is calculated. The coupling of the two QWs starts below 3 nm barrier thickness, above this value there is no coupling.

1. Introduction

The group III-nitrides having a high stability against mechanical, thermal, and chemical stress can be used for light emission and harvesting devices in tough environments and in high power electronics. In addition, GaN/AlN and their compounds have a high conduction band/valence band offset. Thus they are favorable for devices based on intraband transitions like fast modulators, THz devices, and fast photo detectors.[1] The large band offset enables the usage of intraband transitions in the range of 1.55 μm (optical C-band)[2] desired for telecommunication devices. Furthermore $Al_xGa_{1-x}N$ as a ternary alloy allows for another degree of freedom and is used for bandgap adjustment as well as for a tuning of the necessary quantum well (QW) energy levels. For new devices like quantum cascade lasers coupling effects play an important part and the carrier transfer as well as the lifetimes of the charge carriers. Time dependent photoluminescence measurements are important for investigating these effects.

The group III-nitrides are mainly grown in the hexagonal phase, which endures a tilting of the bands caused by internal polarization field along the c-axis and the quantum confined Stark-effect. Both effects complicate the design of devices for intraband transitions in the hexagonal group III-nitrides further.[3] There exist some semi-polar directions for this hexagonal phase, which are intensively examined.[4] Another method is the growth of the metastable cubic phase along (001) on 3C-SiC substrate. This leads to a significantly suppression of the mentioned effects along the growth axis.[5,6]

In this study we examine the carrier transfer by non-resonant tunneling and the carrier lifetimes in cubic GaN/$Al_xGa_{1-x}N$ asymmetric double quantum wells (ADQWs) by time-resolved photoluminescence measurements (TRPL). The transition energies are calculated theoretically via the Schrödinger-Poisson solver nextnano^3.[7] The intensity ratio of the emission of both QWs is determined via rate equations yielding a good agreement with the experimental data.

T. Wecker, Prof. D. Reuter, Prof. D.J. As
Department of Physics
University of Paderborn
Warburger Strasse 100, 33098 Paderborn, Germany
E-mail: wtobias@mail.uni-paderborn.de

G. Callsen, Prof. A. Hoffmann
Institut für Festkörperphysik
Technische Universität Berlin
Strasse des 17. Juni 135, 10623 Berlin, Germany

DOI: 10.1002/pssb.201700373

2. Experimental Section

2.1. Sample Description

Asymmetric cubic GaN/$Al_xGa_{1-x}N$ double quantum wells with an Al content of $x = 0.64 \pm 0.03$ were grown. As substrate a 10 μm 3C-SiC (001) layer on a 0.5 mm thick Si layer was used. The sample structure can be seen in **Figure 1**. A 100 nm thick c-GaN layer was grown on the 3C-SiC substrate as a buffer layer followed by the ADQW structure. The barrier thickness separating a wide (2.5 nm) quantum well (QW_W) and a narrow (1.35 nm) quantum well (QW_N) was increased from 1 nm to 3 and 15 nm. The ADQW structure is placed between two 50 nm cubic $Al_{0.64}Ga_{0.36}N$ layers. Cubic $Al_xGa_{1-x}N$ above $x = 0.71$[8] becomes an indirect semiconductor. In order to avoid additional

© 2017 WILEY-VCH Verlag GmbH & Co. KGaA, Weinheim

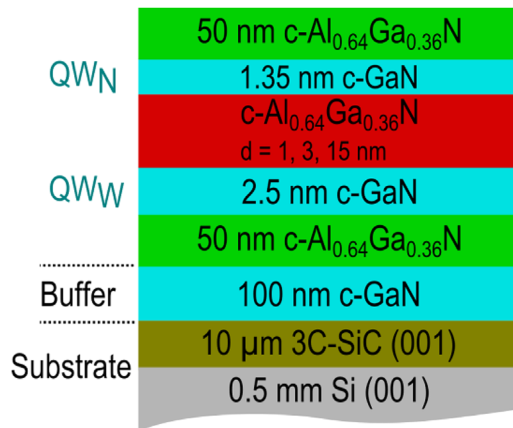

Figure 1. Schematic layer sequence of three samples with a narrow QW (QW_N 1.35 nm) and a wide QW (QW_W 2.5 nm). The AlN barrier between these QWs has been varied as $d = 1$ nm, 3 nm, 15 nm.

effects taking place for the simulations, we kept under this threshold. The applied growth system consists of a Riber-32 radio-frequency plasma-assisted molecular beam epitaxy (PAMBE). For Ga and Al evaporation standard effusion cells were applied. As nitrogen source an Oxford plasma source is used. Reflection high energy electron diffraction (RHEED) is exploited for in situ adjustment of the growth. The best sample qualities for c-GaN can be achieved at a substrate temperature of $T_S = 720\,°C$. Besides one monolayer of Ga excess provide a smoother surface. Further details regarding the growth of cubic nitrides can be found in Ref. [9].

2.2. Nextnano^3 Simulations

The experimental data are compared to simulations of the band structure via a commercial Schrödinger-Poisson solver (nextnano^3[7]). It provides the energy levels of the carriers and the allowed interband transitions. The valence band/conduction band offset ratio at the interface of cubic GaN and cubic $Al_{0.64}Ga_{0.36}N$ is estimated to 79:21.[10]

In the past, quantum well thickness fluctuations in the range of ±1–2 monolayers have been observed. For the cubic GaN one monolayer (1 ML) is 0.225 nm. These fluctuations result in a broadening of the photoluminescence spectra and also in a deviation to the calculated transition energies.

Furthermore nextnano^3 does not include excitonic effects. They are calculated separately and are taken into account afterwards, when comparing with photoluminescence data.[11] Details for the simulations parameters and the exciton treatment can be found in Ref. [12].

3. Results

3.1. Structural Properties

The samples were investigated by high resolution X-Ray diffraction (HRXRD) measurements yielding reciprocal space maps (RSM). An average defect density (mainly stacking faults along (111) planes) in the range of $D = 2 \times 10^{10}\,cm^{-2}$ was determined by the rocking curve full width half maximum (FWHM) in (002) reflection. The Al content of $x = 0.64 \pm 0.03$ was determined exploiting RSM around (113). This also showed the degree of relaxation $R = 0.48 \pm 0.07$ of the layers. The $Al_{0.64}Ga_{0.36}N$ layers are partly tensilely strained in regard to the GaN buffer layer. This leads to an equilibrium lattice parameter in the whole ADQW structure and the QWs are partly compressively strained.

Atomic force microscopy measurements (AFM) provide an rms surface roughness of around 4 nm for $5 \times 5\,\mu m^2$ areas.

3.2. Optical Setups

Time integrated PL measurements were performed with a frequency-quadrupled, picosecond Nd:YAG laser (266 nm, 76 MHz repetition rate). Generally, the samples were situated in a He-flow cryostat (Janis ST-500) reaching a temperature of 7 K. For recording the PL spectra, the luminescence signal was dispersed by a single monochromator (Spex 1702, 1 m focal length, $1200\,g\,mm^{-1}$, 300 nm blaze) and detected by a CCD. For the time-resolved measurements, the luminescence signal was analysed with a subtractive double monochromator (McPherson 2035 – 0.35 m focal length, $2400\,g\,mm^{-1}$, 300 nm blaze) and the detection was achieved with a multichannel-plate (MCP) photomultiplier tube (Hamamatsu R3809U-52). The used excitation power is 0.1 mW with a spot diameter of 1 µm. Additionally, the penetration depth of the laser is large enough to excite even the c-GaN buffer layer, which can be seen as a weak luminescence at 3.21 nm in **Figure 2**. Here, the overall time-resolution of the setup is limited by the laser pulse width of ≈55 ps. Standard photon counting electronics were applied in order to derive the final histograms based on the time-correlated single photon counting (TCSPC) technique.

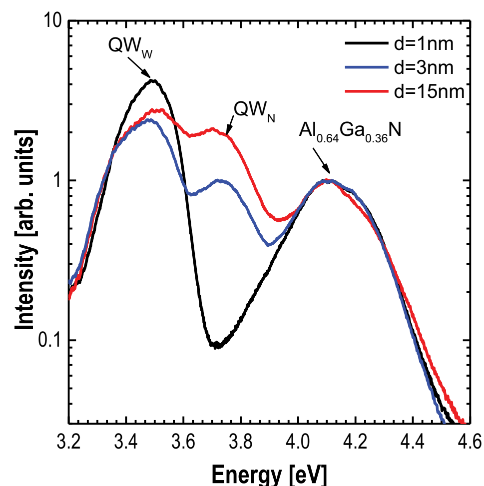

Figure 2. Low temperature (7 K) PL spectra of all three c-GaN/$Al_{0.64}Ga_{0.36}N$ ADQWs in a semi-logarithmic scale. Three emission bands are visible corresponding to the QW_W, the QW_N and the $Al_{0.64}Ga_{0.36}N$ barriers.

© 2017 WILEY-VCH Verlag GmbH & Co. KGaA, Weinheim

3.3. Optical Properties CW

Figure 2 depicts the low temperature interband photoluminescence measurements, in these spectra three emission bands are visible at 3.49, 3.73, and 4.12 eV. These emission bands could be assigned to the wide QW_W, the narrow QW_N and the cubic $Al_{0.64}Ga_{0.36}N$,[8] respectively. In order to compare the PL spectra, they are normalized to the emission of the $Al_{0.64}Ga_{0.36}N$ at 4.12 eV and are plotted in a semi-logarithmic scale. For identical excitation conditions the emission intensity of the QW_N (I_N) becomes weaker and the intensity of the QW_W (I_W) increases for thinner barriers.

3.3. Optical Properties Time-Resolved

A common, convoluted fitting approach[13] was applied to the data, in order to extract all decay times unaffected by the particular temporal response function of the entire setup.

An example of the time transient data is shown in **Figure 3** for the sample with the barrier thickness $d = 15$ nm. This time transient is measured at the emission wavelength for the wide QW (3.49 eV) at 7 K. The red curve is a fit function using a commercial software called Fluofit (Picoquant, GmbH) exploiting a convoluted fitting routine in order to extract the sample emission characteristics:

$$I(t) = \int_{-\infty}^{t} I_{\text{source}}(t') \left(A_{\text{fast}} e^{-\frac{t-t'}{\tau_{\text{fast}}}} + A_{\text{slow}} e^{-\frac{t-t'}{\tau_{\text{slow}}}} \right) dt'. \quad (1)$$

The experimental data are plotted as dots, the blue curve corresponds to the time transient $I_{\text{source}}(t')$ of the laser source and the red curve is the fit curve $I(t)$ as described in Eq. (1). For the best match with the experiment a biexponential decay is assumed. The time transients of the emission for the 3 ADQW samples are shown in **Figure 4** for the QW_W and in **Figure 5** for the QW_N. There is one fast decay time τ_{fast} and a slow component τ_{slow}. Besides the areas A_{fast} and A_{slow} correspond to the intensity.

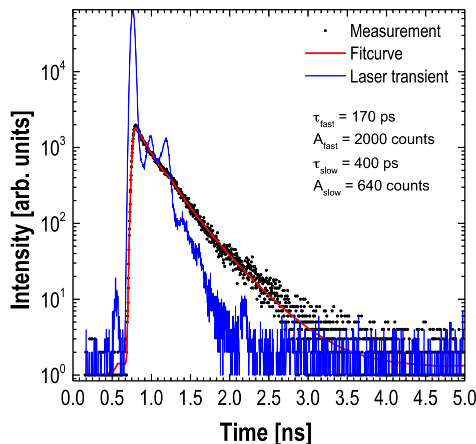

Figure 3. Time transients for the ADQW with the thickest barrier $d = 15$ nm measured at the QW_W (3.49 eV) emission at 7 K. Two decay functions are convoluted with the laser transient to achieve the best fit.

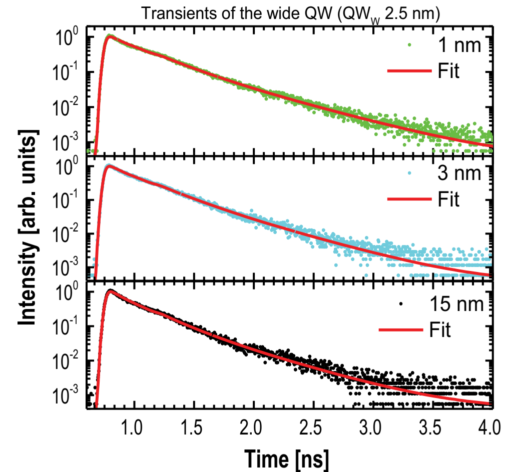

Figure 4. Time transients measured at the QW_W (2.5 nm) emission for the three samples with different barrier thickness d.

The errors for the parameters in **Table 1** and **Table 2** are estimated by fitting several times.

The physical reason for the biexponential transient observed in our sample is up to now unidentified. In literature different explanations are discussed and are mentioned below. There are several papers describing also one fast and one slow decay time in AlGaAs/GaAs structures with an applied electric field. The explanations cover phonon-assisted tunneling and impurity-/defect-assisted tunneling.[14,15] Furthermore the valence band mixing of hh and lh is supposed to influence the tunneling process.[15,16] In addition, it is claimed, that exciton tunneling times are much longer than the tunneling times of individual electrons and holes causing two different decay times.[15,16]

Another approach is to distinguish between direct excitons and spatial indirect excitons (also called crossed excitons) in multi quantum well structures. Due to the tunneling process some of the direct excitons become crossed excitons. These are excitons where electron and hole are in different QWs and thus

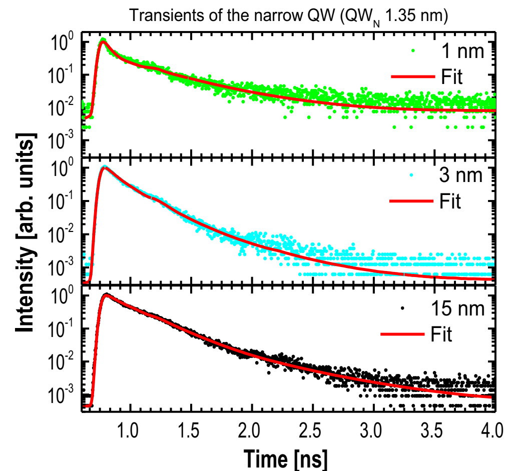

Figure 5. Time transients measured at the QW_N (1.35 nm) emission for the three samples with different barrier thickness d.

 © 2017 WILEY-VCH Verlag GmbH & Co. KGaA, Weinheim

Table 1. Parameter determined at wide QW emission.

Barrier thickness	τ_{fast} [ps]	A_{fast} [counts]	τ_{slow} [ps]	A_{slow} [counts]
1 nm	220 ± 10	3720 ± 90	480 ± 30	1250 ± 90
3 nm	200 ± 10	1800 ± 90	440 ± 30	620 ± 90
15 nm	170 ± 10	2000 ± 90	400 ± 30	640 ± 90

separated by the barrier. The binding energies of crossed excitons are considerably smaller leading to a much lower recombination probability.[16,17] Finally experiments with hydrostatic pressure indicated the participation of Γ-X scattering in the fast decay time and the X–X scattering in the slow decay time.[18] These two decay times have also been reported for other material systems. For example in a report on CdTe/(Cd,Zn)Te asymmetric double QWs the authors explain the slow decay time with the process where the QWs get into thermal equilibrium after excitation.[19] In InGaN/GaN double QWs the slow component has been attributed to impurity related transitions.[20,21]

In our opinion the reason for the biexponential decay originates from the participation of defects in the tunneling process as described in Refs. [14,15].

In the following, we will mainly focus on the fast decay component that dominates the overall intensity in contrast to its slow counterpart.

4. Discussion

For $Al_{0.64}Ga_{0.36}N$ and GaN the effective masses of electrons and heavy holes deviate by a factor of 4.5. This is counteracted by a 4 times higher barrier potential of the electrons. Thus the magnitude of the electron and hole tunneling rates are similar in our cubic samples, so photo-induced space charge built-up effects are assumed to be insignificant compared to asymmetric InGaAs/InP QWs.[22]

The intensities can be expressed by a formalism of non-resonant tunneling rates $T(d)$ for electrons and holes depending on the barrier thicknesses d.[23] For the calculations we use the following model:

Carriers are created by the excitation source in the two QWs and the AlGaN barriers. This is described by generation rates G_W and G_N. These carriers will diffuse to the lowest energy level, so they will recombine in the two QWs (QW_W and QW_N). For coupled QWs a part of the generated electrons in the QW_N is tunneling through the barrier into the wide well with he tunneling rate $T(d)$. The remaining carriers recombine with lifetime τ_N by emitting a photon. This leads to the following rate equation of carrier densities in the narrow n_N and the wide n_W QW:

Table 2. Parameter determined at narrow QW emission.

Barrier thickness	τ_{fast} [ps]	A_{fast} [counts]	τ_{slow} [ps]	A_{slow} [counts]
1 nm	60 ± 10	640 ± 90	450 ± 30	130 ± 90
3 nm	130 ± 10	2460 ± 90	500 ± 30	70 ± 90
15 nm	200 ± 10	2970 ± 90	560 ± 30	200 ± 90

$$\frac{dn_N}{dt} = G_N - \frac{n_N}{\tau_N} - T(d)n_N, \tag{2}$$

$$\frac{dn_W}{dt} = G_W - \frac{n_W}{\tau_W} + T(d)n_W. \tag{3}$$

These formulas are similar for holes.[23] Exploiting the steady state solutions of these formulas, the ratio of the intensities I_N to I_W is

$$\frac{I_N}{I_W} = \frac{\frac{\tau_W}{\tau_N}}{\left(1 + \frac{G_W}{G_N}\right)\tau_W T(d) + \frac{G_W \tau_W}{G_N \tau_N}}, \tag{4}$$

where τ_W and τ_N are the radiative lifetimes in the two QWs. The ratio of the generation rates is a fit parameter. In order to match the experiment for the uncoupled QW with $d = 15$ nm the value of $\frac{G_W}{G_N} = 0.707$ was used. The lifetimes measured by TRPL and the fitted $\frac{G_W}{G_N}$ have been inserted into equation (4) to get **Figure 7**.

The fast decay times (**Figure 6**) clearly depend on the barrier thickness d. For the sample with the thickest barrier the decay time for the wide well starts with 170 ps (blue curve). This value increases for thinner barriers to 215 ps. Furthermore the decay time of the narrow well begins at 202 ps and decreases for thinner barriers to 63 ps (black curve). For thinner barriers the charge carriers of the narrow well tunnel into the wide well, thus the photoluminescence intensity of the narrow well decreases faster. In addition these carriers cause in the wide well more luminescence and the time decay gets slower due to the increased tunneling rate. This is a strong hint for the presence of coupling. Besides the decay time of the QWN and QWW are very similar. Considering the deviation in the fitting as can be seen in Table 1 and Table 2, they are nearly the same. Thus we expect the value of 170 to 200 ps is very close to the decay time of a single QW.

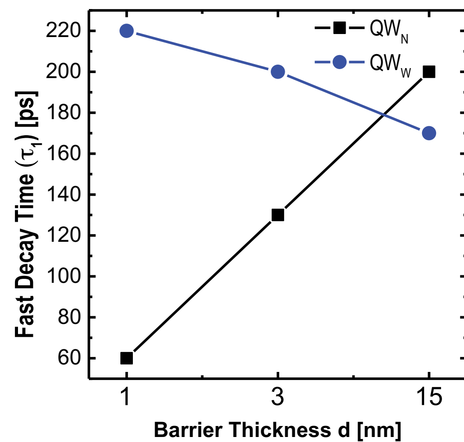

Figure 6. Decay time τ_{fast} of the QW_N (black) and QW_W (blue) emission corresponding to the barrier thickness d for low temperatures (7 K). The decay time increases for the wide QW due to additional electrons of the narrow QW for thinner barriers. The opposite behavior takes place for the narrow QW.

© 2017 WILEY-VCH Verlag GmbH & Co. KGaA, Weinheim

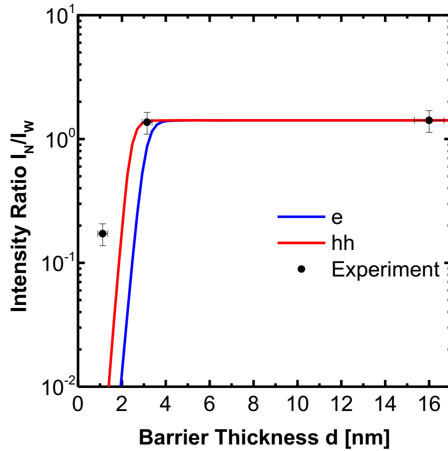

Figure 7. Intensity ratio I_N/I_W as a function of barrier thickness d for low temperatures (7 K). The full dots represent the experimental intensity ratios and the straight lines correspond to the calculated ratios for e (blue) and hh (red).

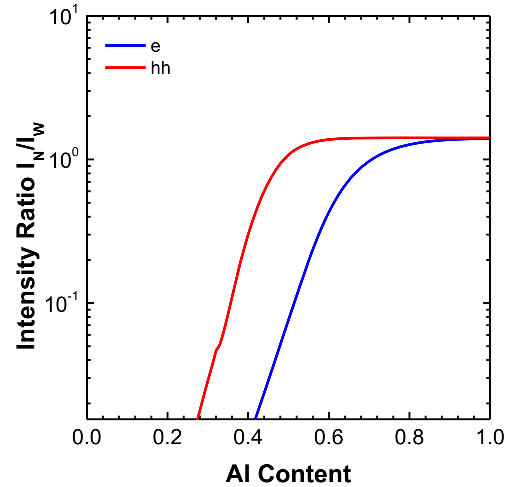

Figure 8. Calculated intensity ratio for the ADQW structure (Figure 1) with a barrier thickness of 3 nm for different Al content at low temperatures.

For barriers thinner than 3 nm the QWs are coupled, as can be seen in Figure 7. The intensity ratio of the luminescence of both QWs is plotted for different barriers d. For this calculation the band structure simulated via nextnano^3 is used. For $d > 3$ nm a constant I_N to I_W ratio is found. This is expected to indicate no coupling between the QWs. The red curve shows the carrier transfer process of the heavy holes and the black one indicates the electron transfer. Only for thinner barriers a deviation to the experimental data (black points) is observed, so a lower carrier transfer is measured. This difference of theory and experiment can be explained by the parameters used for the calculation. For example the uncertainty of 5% for the conduction band/valence band offset at the GaN/AlGaN interfaces and the uncertainty of the Al content in the AlGaN barriers of $x = 0.64 \pm 0.03$. Furthermore, the transfer time is increased due to scattering of carriers by defects in the barriers and lead to a higher I_N to I_W ratio.

The carrier transfer rate for the narrow QW is $r^{narrow}_{transfer} = 1.2 \times 10^{10}\,s^{-1}$ and for the wide QW one obtains $r^{wide}_{transfer} = 1.3 \times 10^{9}\,s^{-1}$ if the coupled (1 nm) and the uncoupled (15 nm) case are compared according to:

$$r^{narrow}_{transfer} = \frac{1}{60\,ps} - \frac{1}{200\,ps}, \tag{5}$$

$$r^{wide}_{transfer} = \frac{1}{170\,ps} - \frac{1}{220\,ps}. \tag{6}$$

The simulated tunneling rates are on the order of $r^{coupled}_{tunnel} = 1 \times 10^{13}\,s^{-1}$ for the coupled ($d = 1$ nm) and $r^{uncoupled}_{tunnel} = 1 \times 10^{-15}\,s^{-1}$ for the uncoupled case ($d = 15$ nm). The difference between experiment and theory is caused by additional effects like the non-radiative recombination and the scattering at defects leading to reduced transfer rates. However, it is already reassuring that the transfer rate probed by the narrow QW exceeds the value obtained for the wide QW. Hence, the wide QW transfer rate of $r^{wide}_{transfer} = 1.3 \times 10^{9}\,s^{-1}$ represents the closest approximation of the effective inter-QW tunneling rate, only limited by the above mentioned material imperfections.

Previous investigation on a similar ADQW structure with an Al content of 0.26 revealed coupling to start at 5 nm thick barriers.[24] For our samples the Al content is with 0.64 much higher, leading to a greater potential offset at the GaN/AlGaN interface. Thus the coupling starts for thinner barriers (below 3 nm). To investigate this in more detail the intensity ratio of the same ADQW (Figure 1) structure with a barrier thickness of 3 nm was calculated. Only the Al content of the barriers was varied leading to **Figure 8**. In this figure the Al content for a 3 nm thick barrier can be seen, where the coupling starts. For this structure this takes place at an Al content below 0.4. This matches with our measured data in Figure 7, where the intensity drop is below 3 nm for an Al content of 0.64. Furthermore the electron tunneling rate is higher than for the heavy holes, thus the radiative recombination is limited by the heavy hole tunneling.[25]

In addition, AlGaN gets indirect for Al higher 0.71.[8] In our first approach this effect has not been included, because the Al content is below $x = 0.71$. Otherwise the change from direct to indirect semiconductor has to be considered for the nextnano^3 simulations and for the tunneling rates as explained in Ref. [26]. Nevertheless our simple model enables a prediction on the coupling for new sample structures with different Al content in the AlGaN barriers up to $x < 0.71$.

5. Conclusion

The carrier transfer by non-resonant tunneling in asymmetric double quantum wells is studied by time-resolved photoluminescence. Asymmetric cubic GaN/$Al_xGa_{1-x}N$ double quantum wells having $x = 0.64 \pm 0.03$ were grown on 3C-SiC (001) substrate by radio-frequency plasma-assisted molecular beam epitaxy. The barrier thickness d between a wide QW (2.5 nm) and

© 2017 WILEY-VCH Verlag GmbH & Co. KGaA, Weinheim

a narrow QW (1.35 nm) is varied from 1 nm, 3 nm to 15 nm. The coupling between the QWs was studied by interband photoluminescence spectroscopy at low temperatures (7 K). Three clearly distinguishable emission bands at 3.49, 3.73, and 4.12 eV are detected and match with the expected values of the different layers. For a decreasing barrier thickness *d* the photoluminescence emission from the narrow QW is significantly supressed, indicating coupling processes. Furthermore two decay times are extracted from the time-resolved measurements. The fast decay time correlates strongly with the barrier thickness *d*. For thinner barriers the decay time of the wide well increases due to additional electrons of the narrow well. The opposite behavior is found for the narrow well. The emission energies for the QWs are in agreement with the theoretical calculations using a Schrödinger-Poisson solver based on an effective mass model (nextnano[3]). The PL intensity ratio of the narrow QW to the wide QW emission for different barrier thicknesses was calculated considering rate equations, providing coupling to start below 3 nm barriers. Furthermore a prediction for different Al content up to 0.71 in the barriers was made, revealing an agreement with the experiment.

Acknowledgements

This investigation was supported financially by the Deutsche Forschungsgemeinschaft (DFG) via TRR142, via the Collaborative Research Centre (CRC) 787 and by the Centre for Optoelectronics and Photonics Paderborn (CeOPP).

Conflict of Interest

The authors declare no conflict of interest.

Keywords

III-nitride semiconductors, charge carrier transfer, cubic crystals, double quantum wells, time-resolved photoluminescence, tunneling

Received: July 18, 2017
Revised: August 2, 2017
Published online: November 28, 2017

[1] H. Machhadani, M. Tchernycheva, L. Rigutti, S. Saki, R. Colombelli, C. Mietze, D. J. As, F. H. Julien, *Phys. Rev. B* **2011**, *83*, 075313.
[2] C. Gmachl, H. M. Ng, *Electron. Lett.* **2003**, *39*, 567.
[3] M. Beeler, C. Bougerol, E. Bellet-Amalaric, E. Monroy, *Phys. Status Solidi A* **2014**, *211*, 761.
[4] F. Scholz, *Semicond. Sci. Technol.* **2012**, *27*, 024002.
[5] D. J. As, C. Mietze, *Phys. Status Solidi A* **2013**, *210*, 474.
[6] C. Mietze, M. Bürger, S. Sakr, M. Thernycheva, F. H. Julien, D. J. As, *Phys. Status Solidi A* **2013**, *210*, 455.
[7] S. Birner, S. Hackenbuchner, M. Sabathil, G. Zandler, J. A. Majewski, T. Andlauer, T. Zibold, R. Morschl, A. Trellakis, P. Vogl, *Acta Phys. Polon. A* **2006**, *110*, 111.
[8] M. Landmann, E. Rauls, W. G. Schmidt, M. Röppischer, C. Cobet, N. Esser, T. Schupp, D. J. As, M. Feneberg, R. Goldhahn, *Phys. Rev. B* **2013**, *87*, 195210.
[9] J. Schörmann, S. Potthast, D. J. As, K. Lischka, *Appl. Phys. Lett.* **2007**, *90*, 041918.
[10] M. Landmann, private communication, **2016**.
[11] H. Mathieu, P. Lefebvre, P. Christol, *Phys. Rev. B* **1992**, *46*, 4093.
[12] T. Wecker, G. Callsen, A. Hoffmann, D. Reuter, D. J. As, *Jpn. J. Appl. Phys.* **2016**, *55*, 05FG01.
[13] D. V. O'Connor, W. R. Ware, J. C. Andre, *J. Phys. Chem.* **1979**, *83*, 1333.
[14] D. Y. Oberli, J. Shah, T. C. Damen, J. M. Kuo, J. E. Henry, J. Lary, S. M. Goodnick, *Appl. Phys. Lett.* **1990**, *56*, 1239.
[15] H. W. Liu, R. Ferreira, G. Bastard, C. Delalande, J. F. Palmier, B. Etienne, *Appl. Phys. Lett.* **1989**, *54*, 2082.
[16] R. Ferreira, P. Rolland, P. Roussignol, C. Delalade, A. Vinattieri, L. Carraresi, M. Colocci, N. Roy, B. Sermage, J. F. Palmier, B. Etienne, *Phys. Rev. B* **1992**, *45*, 11782.
[17] F. C. Michl, R. Winkler, U. Rössler, *Solid State Commun.* **1996**, *99*, 13.
[18] M. Nido, M. G. W. Alexander, K. Reimann, K. Ploog, W. W. Rühle, *Surf. Sci.* **1990**, *229*, 195.
[19] S. Haacke, N. T. Pelekanos, H. Mariette, M. Zigone, A. P. Heberle, W. W. Rühle, *Phys. Rev. B.* **1993**, *47*, 24.
[20] M.-Y. Ryu, P. W. Yu, E.-J. Shin, J. I. Lee, S. K. Yu, E. S. Oh, Y. J. Park, H. S. Park, T. I. Kim, *J. Korean Phys. Soc.* **2000**, *37*, 387.
[21] E.-J. Shin, N. W. Song, J. I. Lee, D. Kim, M. Y. Ryu, P. W. Yu, D. Lee, Y.-H. Choi, C.-H. Hong, *J. Korean Phys. Soc.* **1990**, *34*, 374.
[22] R. Sauer, K. Thonke, W. T. Tsang, *Phys. Rev. Lett.* **1988**, *61*, 609.
[23] T. Tada, A. Yamaguchi, T. Ninomiya, H. Uchiki, T. Kobayashi, T. Yao, *J. Appl. Phys.* **1988**, *63*, 5491.
[24] T. Wecker, F. Hörich, M. Feneberg, R. Goldhahn, D. Reuter, D. J. As, *Phys. Status Solidi B* **2015**, *252*, 873.
[25] K. Mizutani, Y. Nishimoto, M. Yamaguchi, N. Sawaki, H. S. Ahn, *J. Korean Phys. Soc.* **2003**, *42*, 633.
[26] E. E. Mendez, E. Calleja, W. I. Wang, *Phys. Rev. B* **1986**, *34*, 8.

© 2017 WILEY-VCH Verlag GmbH & Co. KGaA, Weinheim